Synthesis, Multi-Identifications of Some Complexes with a Newly Ligand (4-FADPD) Derived from Caffeine and Evaluation of the Anticancer Activity of Au(III) Nano-Complex

Majida Ibrahim Obaid[1], Ibtihal Kadhim Kareem[1*], and Wurood Ali Jaafar[2]

[1]*Department of Chemistry, Faculty of Education for Women, Kufa University, Najaf 54001, Iraq*

[2]*Department of Chemistry, College of Education for Pure Science (Ibn Al-Haitham), University of Baghdad, Adamiyah, P.O. Box 4150, Baghdad, Iraq*

** **Corresponding author:***

email: ibtihal.dosh@uokufa.edu.iq

Received: September 4, 2025
Accepted: January 21, 2026

DOI: 10.22146/ijc.110949

Abstract: *A novel ligand ((1E)-(2-(4-fluorobenzylidene)amino)methyl) phenyl)diazenyl)-1,3,7-trimethyl-3,7-dihydro-1H-purine-2,6-dione (4-FADPD) was synthesized via the azotization reaction of 2-aminobenzylamine with caffeine, and the resultant compound was condensed with 4-fluorobenzaldehyde to form a newly azo-Schiff base ligand. Its complexes with Cu(II), Ag(I), and Au(III) were synthesized. The results of multi-identifications, including XRD, elemental analysis (C.H.N), UV-vis spectroscopy, FTIR, and ^{1}H-NMR, were used to propose the suggested structures using molar conductivity measurements. These data were utilized to propose appropriate geometric configurations for all complexes. The azo-Schiff base ligand coordinates toward the Cu(II) ion in octahedral geometry and Ag(I) ion in tetrahedral geometry, whereas the Au(III) ion gives it a square planar structure. Nanoparticle size was determined using scanning microscopy (FE-SEM). Significant antiproliferative activity was observed with the Au(III) nanocomplex against human lung cancer (A549) cells, compared with normal cell lines (HDFn), as indicated by the IC_{50} values. The purpose of our research is to prepare new nanocomplexes derived from caffeine and to demonstrate the effectiveness of an Au(III) nanocomplex against lung cancer as a future treatment that may benefit pharmaceutical preparations.*

Keywords: *gold nano-complex; lung cancer; caffeine; anticancer activity*

■ INTRODUCTION

Transition metal complexes play a pivotal role in medicinal biochemistry, contributing to the treatment of various human ailments such as cancer [1]. Purine bases, such as xanthine derivatives, are known to multitarget and operate as non-selective agents of a variety of cellular proteins [2]. Certain xanthine derivatives function as diuretics [3], lipolysis agents [4], analgesic adjuvants [5], and as bronchodilators [6] and cognitive enhancers [7]. They are also used to treat cerebral ischemia [8], Parkinson's disease [9], and renal failure [10]. Additionally, the efficacy of xanthine derivatives as adjuvants for cancer chemotherapy has been investigated [11]. Caffeine can form complexes with various acidic drugs, thereby modifying their pharmacokinetic properties [12]. Additionally, caffeine has demonstrated anticancer activity, both individually and in combination with anticancer drugs [13]. Caffeine is present in several over-the-counter analgesics. It has many well-documented drug-drug and drug-food interactions [14]. It has been demonstrated that methylxanthines generally exhibit inhibitory effects on several antimicrobial agents [15].

Azo-imine derivatives are chemical compounds that have attracted significant attention in scientific research, distinct from imine compounds and azo dyes [16]. Due to the presence of two reactive functional groups, N=CH and N=N [17], these compounds are used as ligands in coordination chemistry and can coordinate in a wide range of ways. They may be coordinated through the nitrogen atoms of the azo and imine groups [18], or by the nitrogen of the azo group

alone, and they can ultimately coordinate through the azo-imine nitrogen atoms [19].

Azo-Schiff compounds find various applications in daily life [20-21], as they are used for corrosion inhibition in manufacturing [22], antioxidants [23], nuclear waste disposal [24], and the manufacture of plastics, leather, and textiles [25]. Complexes of azo-Schiff bases have demonstrated their value as antifungals and anticancer agents [26] and as antimicrobial agents [27]. Over the past few decades, transition-metal complexes have been used to treat a wide range of illnesses, including inflammation, bacterial infections, and cancer [28]. Since cancer is a complex and multigenetic illness, metal complexes exhibiting a single anticancer mechanism are usually ineffective in treating tumors and may result in medication toxicity and resistance [29]. Therefore, it is ideal to develop multi-targeted anticancer drugs to avoid these side effects and multidrug resistance [30]. To overcome the limitations of single-targeting medications, multitargeting medications are currently in high demand [31]. It is possible to construct transition metal complexes as multi-targeted anticancer agents [32]. Our research aims to synthesize and characterize a novel azo-Schiff base ligand (L) derived from caffeine and investigate its transition metal complexes, where Cu(II), Ag(I), and Au(III) complexes have been prepared with the ligand ((1*E*)-(2-(4-fluorobenzylidene) amino)methyl)phenyl)diazenyl)-1,3,7-trimethyl-3,7-dihydro-1*H*-purine-2,6-dione, derived from xanthine compounds. The effect of the Au(III) nanocomplex on lung cancer cells (A549) was studied and compared with healthy cells (HDFn), demonstrating high effectiveness in preventing A549 cancer cells while remaining cell-safe for intact HDFn.

■ EXPERIMENTAL SECTION

Materials

The materials: 2-amino benzylamine (98%), silver nitrate (99%), and hydrochloric acid (12 M) were acquired from the English company Sigma Aldrich; 4-fluoro benzaldehyde (99%) was obtained from Fluka; copper(II) chloride dihydrate (99%) and gold sodium chloride(III) (98%) were acquired from Macklin; methanol (99%) and benzene (99%) were obtained from G.C.C. Company; absolute ethanol (99%) was obtained from Sharlut Company; and dimethyl sulfoxide (DMSO, 98%) was obtained from A.C.S. Company. Glacial acetic acid (99%) was obtained from Merck. All these chemicals were used as received, without any further purification.

Instrumentation

The instrumentation used was as follows: melting points were measured using a Type Shanghai Drawell Scientific Instrument for the ligand and its complexes. ^{1}H-NMR spectra were acquired as solutions in DMSO-d_6 solvent using a Varian 500 MHz spectrophotometer, while the mass spectra (MS) were recorded on a GC-MS-QP2010SE: Shimadzu Spectrometer. The Shimadzu UV-160PC Visible-UV spectrophotometer was used for recording UV-vis spectra. Magnetic susceptibility measurements were performed using the Faraday method with a balanced magnet (MSB-MKI). Infrared (IR) spectra were measured using a Shimadzu FTIR-8400 spectrometer utilizing KBr in the 4000–400 cm^{-1} wavelength range. C.H.N elemental analysis was conducted using a C.H.N elemental analyzer (EURO 2012 EA 300). A field-emission scanning electron microscope (FESEM) was used to determine the percentage of metals in the complexes. A highly magnified image (120.00 kX) was obtained using a TESCAN (Germany) microscope. X-ray diffraction (XRD, Bruker, Germany) was used for recording XRD patterns. The manufacturer names, countries, and types of equipment used for toxicological studies were as follows: Eppendorf (Germany) centrifuge cooling; Olympus (Japan) inverted microscope; Gallenkamp (England) CO_2 incubator; K and K (Korea) laminar air flow; Bio-Rad (Germany) microtiter plate reader; Sartorius (Germany) sensitive balance; Sigma (USA) haemocytometer; and ThermoFisher (Japan) ELISA reader.

Procedure

Synthesis of 4-FADPD

The 4-FADPD was created in two steps. The first step involved reacting diazonium salt with a suitable amount of caffeine in an alkaline medium. The diazonium solution was prepared by dissolving 0.01 mol (1.22 g) of 2-aminobenzylamine in 30 mL of deionized water and

3 mL of concentrated HCl with continuous shaking. The solution of $NaNO_2$ (0.01 mol, 0.7 g) was prepared in 5 mL of ice-cold deionized water. It was added to the diazonium solution dropwise, with stirring and shaking to complete the diazotization at 0–5 °C, and then left to stand for 30 min. This diazonium solution was added dropwise to 0.01 mol (1.94 g) of caffeine dissolved in 50 mL of absolute ethanol and 50 mL of 40% $NaHCO_3$ solution at 0–5 °C. The color slowly changed to orange, which indicates the coupling process had occurred between the two solutions. The synthesis of azo compounds was followed by neutralization using dilute HCl until the pH reached ~7.5. The mixture formed was left for 24 h, filtered, and washed carefully with deionized water [33].

In the second step, the new azo-Schiff base ligand - ((1*E*)-(2-(4-8-fluorobenzylidene)amino)methyl)phenyl) diazenyl)-1,3,7-trimethyl-3,7-dihydro-1*H*-purine-2,6-dione was prepared by dissolving 4-fluorobenzaldehyde (3 mmol, 0.37 g) in 10 mL of absolute ethanol. After 2 min of stirring, 3 drops of glacial acetic acid were added, and the mixture was left at room temperature for 5 min. Then (3 mmol, 1.04 g) of azo dye was dissolved in 10 mL of absolute ethanol, slowly added, and the solution was heated to 78 °C for 16 h to obtain the new ligand. The product obtained was cooled, dried, and then recrystallized using hot absolute ethanol [34]. Table 1 lists the physical attributes, and Scheme 1 outlines the procedures for preparing this ligand.

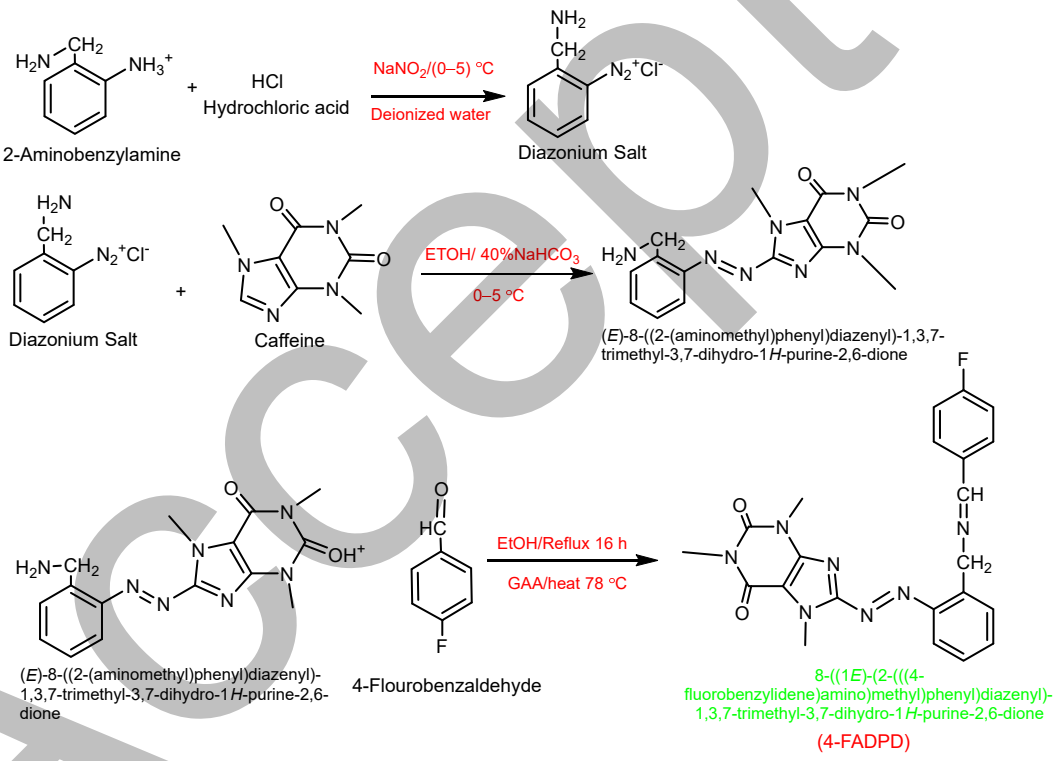

Scheme 1. Synthesis of a new azo-Schiff base ligand(4-FADPD)

Table 1. The ligand (4-FADPD) and its metal complexes' physical characteristics

Chemical formula	Color	M.Wt (g/mol)	M.p. (°C)	Yield%
$C_{22}H_{20}FN_7O_2$	Brown	433.45	80–82	69%
$[Cu(C_{22}H_{20}FN_7O_2)Cl_2{\cdot}H_2O]$	Dark brown	585.99	188–190	95%
$[Ag(C_{22}H_{20}FN_7O_2)H_2O]NO_3$	Olive	621.31	148–150	91%
$[Au(C_{22}H_{20}FN_7O_2)Cl]Cl_2{\cdot}H_2O$	Dark brown	754.92	246–248	96%

Synthesis of Cu(II) and Ag(I) metal complexes

Two metal complexes were produced by combining 0.0004 mol of $CuCl_2 \cdot 2H_2O$ in 10 mL ethanol with 15 mL absolute ethanol solution of (0.4 mmol, 0.2 g) of the new ligand in a 1:1 ratio (metal:ligand) to form the Cu(II) complex, and by mixing 0.4 mmol of $AgNO_3$ in 10 mL ethanol with 15 mL absolute ethanol solution of (0.4 mmol, 0.2 g) of the new ligand in a 1:1 ratio (metal:ligand) to form the Ag(I) complex. The resulting mixtures were refluxed for 3 h in both cases. The products obtained were cooled, dried, and recrystallized using hot absolute ethanol.

Preparation of nano-gold complex $[AuLCl]Cl_2 \cdot H_2O$

The preparation of $[AuLCl]Cl_2 \cdot H_2O$ involved adding 0.6 mmol (0.21 g) of $NaAuCl_4$ in 10 mL of absolute ethanol to a 1:1 (M:L) molar ratio solution containing 0.3 g (0.6 mmol) of L. The resulting solution was refluxed for 25 h at 78 °C. The product obtained was cooled, dried, and recrystallized using hot absolute ethanol. The physical characteristics of these complexes are listed in Table 1, while Scheme 2 shows the steps for their preparation.

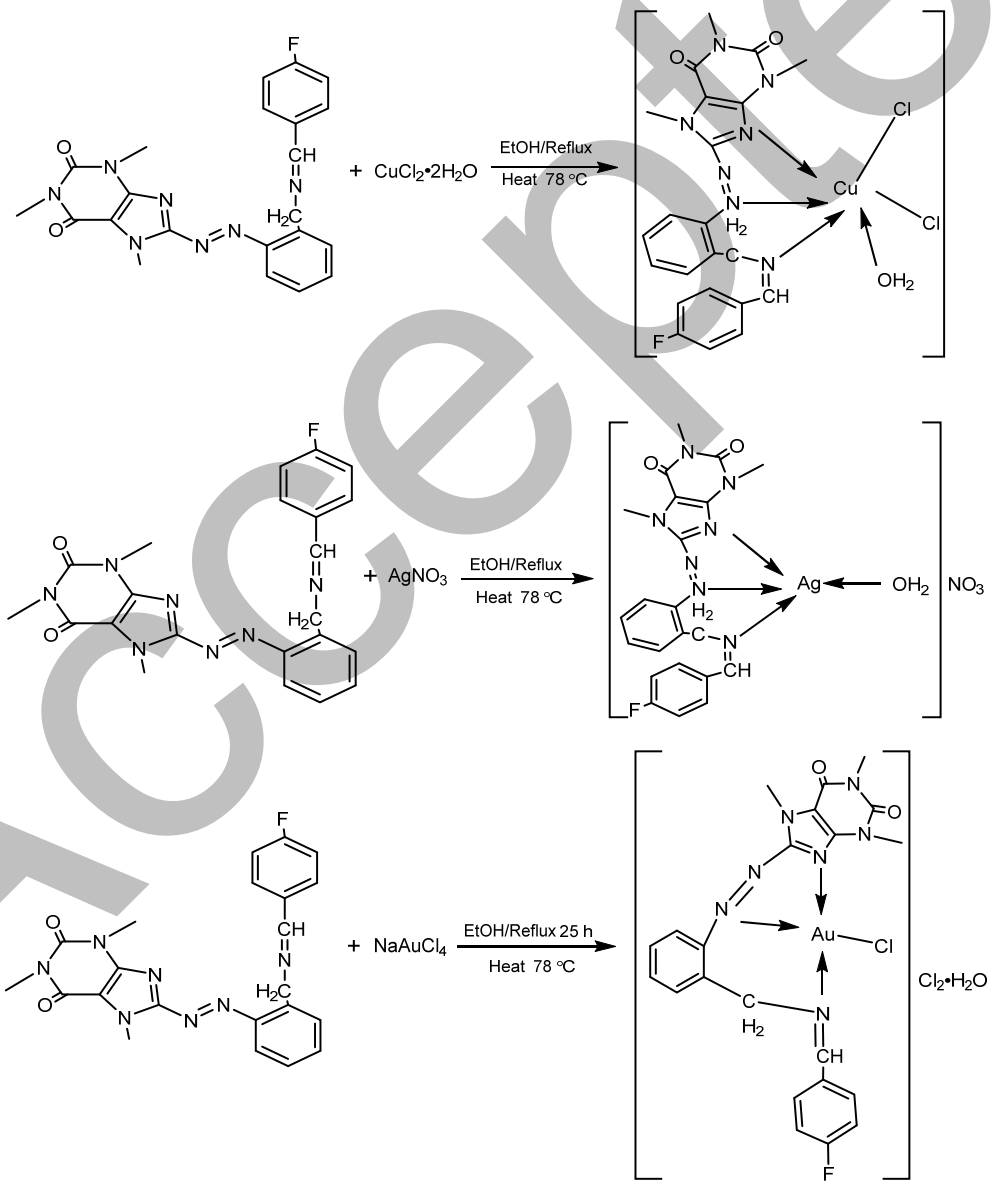

Scheme 2. Synthesis of novel metal complexes with the ligand (4-FADPD)

In vitro *Au(III) nano-complex cell cytotoxicity and viability assays*

The gold nano-complex showed a toxic effect on lung cancer cells. To prepare the cancerous and healthy cell lines for the study, the A549 cell line was derived from lung tissue obtained from a white male patient with lung cancer, aged 58. This cell line can be used in research on cancer, immuno-oncology, and toxicity. The dermal fibroblast primary human, neonatal (HDFn), is a normal cell line derived from newborn foreskin. It has been used in studies on pathogen response, skin aging, wound healing, gene delivery, and skin conditions like scleroderma. These cell lines were obtained from the Pharmacology Department, College of Medicine, University of Malaya, Kuala Lumpur, Malaysia. The cytotoxic effect of the $[AuLCl]Cl_2{\cdot}H_2O$ nano-complex was evaluated using an Intron Biotech MTT ready-to-use kit, and several concentrations were tested.

Protocol

In 96 flat-bottom microtiter plates, tumor cells (10^4–10^6 cells/mL) were cultivated in a final volume of 200 µL of full culture media in each well. After covering the microplate with sterile Parafilm, it was carefully shaken. The plates were incubated for 24 h at 37 °C with 5% CO_2. Following incubation, the medium was removed, and the wells were filled with two-fold serial dilutions of the compounds (400, 200, 100, 50, and 25 µg/mL). Both the controls (cells treated with serum-free media) and each concentration were utilized in triplicate. For a chosen exposure duration of 4 h, plates were incubated at 37 °C with 5% CO_2.

For 24 h, 20 µL of each compound was added to each well. Each well received 10 µL of the MTT solution upon exposure. The plates were then incubated for 4 h at 37 °C with 5% CO_2. After carefully removing the media, 100 µL of solubilization solution was added to each well and incubated for 5 min. An ELISA reader operating at 575 nm was used to measure the absorbance. The Eq. (1) was used to statistically analyze the optical density data and determine the concentrations of chemicals required to reduce cell viability by 50% for each cell line [35].

$$Y = D + \frac{A - D}{1 + 10^{(x - \log C)B}} \quad (1)$$

■ RESULTS AND DISCUSSION

An excellent solubility in different solvents was observed for the ligand and its metal complexes, such as DMF, DMSO, MeOH, and EtOH. Additionally, they exhibit stability in air. These metal complexes and the ligand were studied using various analytical methods, including elemental analysis, molar electrical conductivity, infrared spectroscopy, UV-vis spectroscopy, MS, and ^{1}H-NMR (only the ligand was measured). The experimental results and the analytical data from the complexes are in good accord, confirming their accuracy.

Based on the data shown in Table 2, specifically the results of precise elemental analysis (C.H.N) and molar conductivity measurements, it was determined that the molar ratio adopted was 1:1 (M:L) for the Cu(II) and Ag(I) complexes, where the tridentate ligand coordinates with the metal ions through three sites (N,N,N) to form an octahedral geometry in the Cu(II) complex and a tetrahedral geometry in the Ag(I) complex. Meanwhile, in the Au(III) Nano-complex, the

Table 2. Results of the elemental analysis data of 4-FADPD and its metal complexes

Compounds	M.wt. (g/mol)	Found (Calc., %)			
		C	H	N	M
4-FADPD = $C_{22}H_{20}FN_7O_2$	433.45	60.85 (60.90)	4.56 (4.60)	22.55 (22.60)	–
$[Cu(C_{22}H_{20}FN_7O_2)Cl_2H_2O]$	585.99	45.00 (45.05)	3.80 (3.75)	16.68 (16.72)	10.82 (10.84)
$[Ag(C_{22}H_{20}FN_7O_2)H_2O]NO_3$	621.31	42.47 (42.49)	3.50 (3.54)	18.00 (18.02)	17.33 (17.36)
$[Au(C_{22}H_{20}FN_7O_2)Cl]Cl_2.H_2O$	754.92	34.94 (34.97)	2.87 (2.91)	12.94 (12.98)	26.01 (26.09)

tridentate ligand coordinates with the Au(III) ion through the same coordination sites mentioned above, resulting in a square planar geometry with a 1:1 (M:L) molar ratio. Thus, the surrounding ligands coordinate around the core metal ions. This aligns with previous literature on this type of complex [36]. The synthesized chelate complexes Ag(I) and Au(III) in this study exhibited significant conductivity, demonstrating an electrolytic character.

^{1}H-NMR Spectra

The chemical environment of organic molecules can be determined by NMR spectroscopy using tetramethylsilane (TMS) as the internal reference standard [37]. The ligand was analyzed using the ^{1}H-NMR technique with DMSO-d_6 as the solvent (Fig. S1). The spectrum obtained provided reliable data, and the molecular structure was determined from the hydrogen-atom chemical shifts. The spectrum exhibited distinct signals, including a singlet at 2.5 ppm corresponding to the solvent protons [38], and a singlet at 3.40 and 3.88 ppm attributed to the (N–CH_3 purine) group. It also showed a doublet at 3.97 ppm corresponding to the CH_3 proton in the (N–CH_3 imd) group [39]. Also, a singlet appeared at 3.27 ppm, assigned to water protons, and the ligand showed a singlet at 4.70 ppm belonging to the methylene (CH_2) proton. Multiplet signals at 6.35–8.46 ppm were assigned to the aromatic protons. A singlet at 10 ppm indicated the proton of the azomethine (–CH=N) group. As for the complexes, they showed similar signals to the ligand (Fig. S2-S4).

MS

MS is an essential diagnostic tool that allows the molecular weight and molecular formula of new compounds to be confirmed [40]. The MS of the new organic ligand (Fig. S5) and the gold complex (Fig. S6) were measured using mass spectrometry. The spectrum showed the organic ligand molecular ion (m/z^+) at 433.0, and the gold complex molecular ion (m/z^+) was observed at 755.0 [41]. Schemes S1 and S2 show the mass fractionation pathways of ligand and [Au(L)Cl]Cl_2·H_2O complex, respectively.

FTIR Spectra of 4-FADPD and Its Metal Complexes

To identify any changes that may have occurred during the Complexation process, the spectra of the complexes and the free ligand were compared. The formation of the complexes was confirmed by FTIR spectra, which revealed distinct spectral regions in the ligand and the complexes. Several significant bands in the complexes' spectra, including the N=N and C=N bands of the imidazole ring, showed a shift. These bands exhibited variations in position, intensity, and shape. Other new bands in the 400–600 cm^{-1} range indicated the formation of M–N bond types, confirming coordination between the metal and the ligand at the indicated sites, consistent with coordination behavior reported in previously published articles [42-43]. All relevant data are presented in Table 3 and Fig. S7–S10.

Measurement of Molar Conductivity

The results show that the investigated chelate complexes of the metal ions, i.e., [Cu(L)Cl_2·H_2O], [Ag(L)H_2O]NO_3, and [Au(L)Cl]Cl_2·H_2O, had molar electrical conductivities of 19.5, 32.0, and 76.3 cm^2/mol, respectively when measured in solutions containing the

Table 3. The IR spectrum frequencies for the new heterocyclic ligand and its metal complexes

Compound	ν(OH) δ(OH)	ν(C-H) arom	ν(C-H) alpha	ν(C=O)	ν(C=N) Schiff	ν(C=N) imd	ν(N=N)	H_2O coord	(M–N)
4-FADPD $C_{22}H_{20}FN_7O_2$	–	3062 3024	2891 2850	1698	1599	1552	1434	–	–
[Cu(L)Cl_2·H_2O]	3412 1373	3057	2953 2924	1701	1618	1568	1456	929	410–572
[Ag(L)H_2O]NO_3	3412 1382	3061	2922 2850	1701	1616	1544	1454	939	420–516
[Au(L)Cl]Cl_2·H_2O	3414 1400	3045	2922 2850	1693	1616	1573	1452	–	416–596

novel ligand at a concentration of 10^{-1} M per complex. These measurements were conducted at laboratory temperature, with DMSO as the solvent. It can be observed that the Au(III) and Ag(I) complexes exhibit ionic properties, based on the molar conductivity data, whereas the Cu(II) complex is neutral. The results are consistent with findings reported in the literature for ionic metallic compounds [44].

Electronic Spectra

Electronic absorption spectra are valuable for assessing the impacts facilitated through alternative methods of structural investigation. The ligand spectrum in DMSO as a solvent exhibited three absorption peaks at 263 and 299 nm, corresponding to electron transitions of the $\pi\rightarrow\pi^*$ type, and at 347 nm, attributed to an electron transition of the $n\rightarrow\pi^*$ type. The presence of double bonds in the ligand, which are connected to atoms with unshared electron pairs, caused this third peak to be consistent with what was reported by Radhi et al. [44]. The Ag(I) complex spectrum solution shows an absorption peak at 370 nm, due to metal-to-ligand charge transfer (M→L CT). The Cu(II) complex solution spectrum shows an absorption peak at 384 nm, also due to M→L CT, and a peak at 906 nm, assigned to the $^2Eg\rightarrow^2T_2g$ electron transition. This observation aligns with existing research on the occurrence of this band in Ag(I) and Cu(II) complexes with tetrahedral and octahedral geometries, respectively.

As for the electronic spectrum of the Au(III) complex with the ligand, this complex exhibited a band at 906 nm, which was assigned to the $^1A_1g\rightarrow^1A_2g$ transition, and an absorption peak at 660 nm, which has been linked to the $^1A_1g\rightarrow^1B_1g$ electron transition. The Au(III) complex exhibits a diamagnetic moment and a square-planar geometry. Recently, complexes of Au(III) ions have been used in medical applications for cancer treatment, and their importance in this field has increased significantly [46]. The reason is that Au(III) is electronically identical to Pt(II), and Au(III) complexes, which are tetra-coordinated and have a square-planar shape, are similar to cisplatin in both electronic arrangement and geometric structure. The red shift in the complexes is caused by charge transfer from the ligand to the metal (L→M, CT). Table 4 lists the electronic spectra of the new ligand and its complexes in DMSO solvent. Fig. S11–S14 show the electronic spectra of the prepared ligand and its metallic complexes.

FESEM of Complexes

FESEM technology offers a flexible approach to analyzing the surface morphology (particle shape and size) and topography (surface properties) of substances [47-48]. Prior to imaging, a thin layer of material was coated onto the samples, with a 30.00 kV acceleration voltage, a 500 nm cross-sectional distance, and a 120 kX magnification applied.

The Au complexes exhibit crystalline agglomeration, as observed in the FESEM images (Fig. S15). Particle sizes were calculated using ImageJ software. The micrograph of the $[Au(L)Cl]Cl_2{\cdot}H_2O$ complex reveals particles with irregular shapes and an average size of 47.93 nm. These particles have irregular, non-uniform morphology and an average particle size of

Table 4. Geometry, hybridization, and electronic transitions observed for the ligand and its complexes at (10^{-3} M)

Compounds	λ_{max} (nm)	ν (cm^{-1})	Transitions	Geometry	Hybridization
(4-FADPD)	263	38022	$\pi\rightarrow\pi^*$	–	–
$C_{22}H_{20}FN_7O_2$	305	32786	$n\rightarrow\pi^*$		
$[Cu(L)Cl_2{\cdot}H_2O]$	265	37735	Intra ligand	Distorted octahedral	sp^3d^2
	384	26041	M→L, CT		
	906	11037	$^2Eg\rightarrow^2T_2g$		
$[Ag(L)H_2O]NO_3$	271	36900	Intra ligand	Tetrahedral	sp^3
	370	27027	M→L, CT		
$[Au(L)Cl]Cl_2{\cdot}H_2O$	268	37313	Intra ligand	Square planer	dsp^2
	660	15151	$^1A_1g\rightarrow^1B_1g$		
	906	11037	$^1A_1g\rightarrow^1A_2g$		

less than 100 nm. The images reveal that the grain sizes of the synthesized substances are less than 100 nm, placing them in the nanoscale range. This increased surface area enhances the quantitative effect, creating new energy levels that allow electrons to move more freely [49]. The properties of this complex compound make it a promising candidate for medical research, particularly for studying its potential to inhibit various types of cancer.

XRD Diffractograms

XRD provides precise data regarding the molecular or atomic configuration of solid-state materials [50]. The XRD diffractograms were measured for $[Au(L)Cl]Cl_2{\cdot}H_2O$. The Cu Kα radiation was calculated over 0° to 80° in 2θ, with a wavelength of 1.54060 Å and generator settings of 30 mA/40 kV. Using the X'Pert HighScore computer program, many properties of the diffraction spectra can be determined by evaluating the recognized peaks [51]. The results indicated that the compound exhibited a semi-crystalline character (Fig. S16). By applying Bragg's equation [52], we estimated the significant reflections and measured the corresponding d-spacing values.

The equation $n\lambda = 2d\sin\theta$ was used, where d represents the distance between the crystalline layers, and n is an integer (1, 2, 3, ...). The symbol λ represents the wavelength of X-ray Cu Kα (1.540598 Å), and θ represents the diffraction angle. Eq. (2), developed by Debye and Scherrer, was used to determine the average crystallite diameter and its size distribution [53];

$$D = \frac{k\lambda}{\beta\cos\theta} \quad (2)$$

where D represents the crystallite's average diameter, β is the line broadening at half maximum intensity (FWHM), and k is the form factor (0.891) [54].

The XRD spectra demonstrated a clear change in the previously given data, including the spacing between the crystalline levels (d), the crystal size (D), the microductility (ε), and the dislocation density (δ). This confirms the existence of the coordination process. In the metal complexes under investigation, we observed an inverse relationship between D, ε, and δ: as D increases, ε and δ decrease, and thus the crystal defects decrease.

The sharp peaks indicate crystalline or semi-crystalline structures. The intensity of these peaks is determined by the crystal arrangement and the characteristics of the crystal lattice and crystal planes. In addition, the experimental average crystallite size for the reported $[Au(L)Cl]Cl_2{\cdot}H_2O$ complex was 43.2306 nm. The compound exhibits nanostructural properties, as evidenced by its crystalline size being less than 100 nm. These data support our previous FESEM analyses. The crystalline properties of the Au(III) complex are shown

Table 5. The crystalline properties of the Au(III) nano-complex

Compound	Pos. 2θ (°)	Height (cts)	FWHM 2θ (°)	*d*-spacing (Å)	Rel. Int. (%)	Crystallite Size D (nm)	Dislocation density $\delta\times10^{-3}$ (nm)^2	Microstrain $\varepsilon\times10^{-3}$	Average size (nm)
$[Au(L)Cl]Cl_2{\cdot}H_2O$	22.8102	48.87	1.1584	3.89543	1.57	7.21895	19.188	25.0506	43.2306
	27.317	74.33	0.125	3.26212	2.39	67.48696	0.2195	2.24488	
	31.6415	536.11	0.1683	2.82545	17.22	50.62420	0.3901	2.59120	
	32.5747	431.8	0.1866	2.74661	13.87	45.76657	0.4774	2.78680	
	38.1416	3113.34	0.1925	2.35755	100	45.05630	0.4925	2.42977	
	44.3309	1118.8	0.2365	2.0417	35.94	37.42683	0.7138	2.53320	
	45.3835	284.64	0.1849	1.99677	9.14	48.05337	0.4330	1.92937	
	46.779	58.02	0.2354	1.9404	1.86	37.94056	0.6946	2.37502	
	56.3976	94.56	0.1743	1.63015	3.04	53.36340	0.3511	1.41839	
	58.1867	121.33	0.1368	1.58422	3.90	68.57390	0.2126	1.07289	
	64.533	690.66	0.2302	1.44289	22.18	42.11281	0.5638	1.59102	
	75.2352	106.44	0.1232	1.26198	3.42	84.00000	0.1417	0.69751	
	77.4414	177.79	0.2149	1.23144	5.71	48.89071	0.4183	1.16963	
	77.5424	596.95	0.2004	1.23009	19.17	52.46531	0.3632	1.08877	

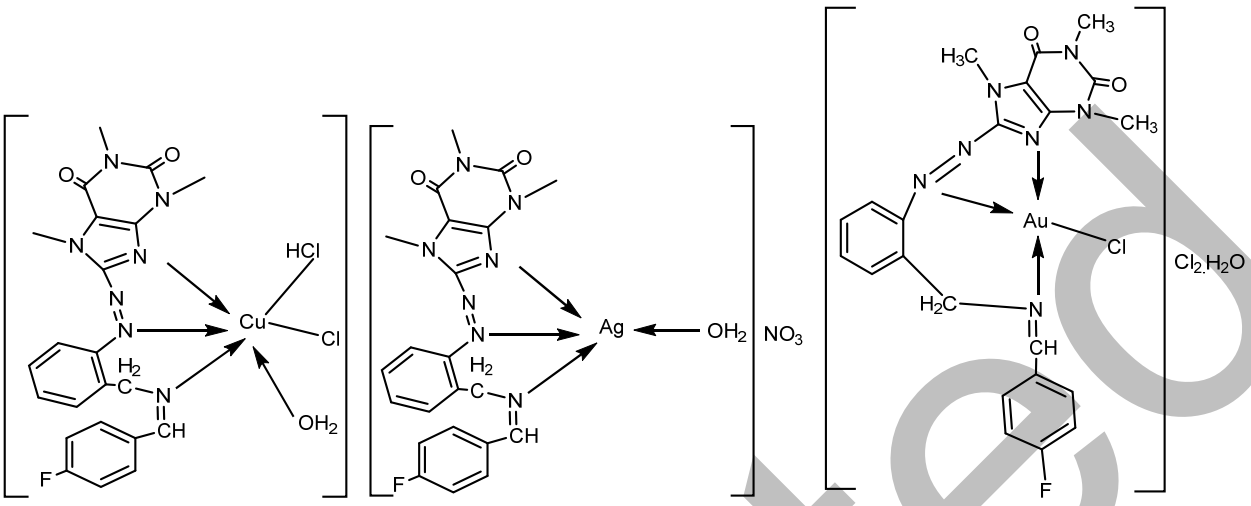

Fig 1. Proposed structure of the metallic complexes

Table 6. The effect of the complex $[Au(L)Cl]Cl_2{\cdot}H_2O$ on A549 cells and comparison with HDFn

Conc. (μg mL^{-1})	Mean percentage (%)			
	Cancer cell lines A549		Normal cell lines HDFn	
	Cell viability	Cell inhibition	Cell viability	Cell inhibition
25	93.71	6.29	96.88	3.13
50	83.22	16.78	95.22	4.78
100	72.03	27.97	93.25	6.75
200	60.22	39.78	83.99	16.01
400	48.30	51.70	72.49	27.51
	IC_{50} = 235.2		IC_{50} = 296.5	

in Table 5 (Fig. S16), which presents the XRD spectra of the Nano $[Au(L)Cl]Cl_2{\cdot}H_2O$ complex. The results indicated octahedral and tetrahedral shapes for the Cu(II) and Ag(I) complexes, respectively, while a square-planar shape was proposed for the gold nanocomplex with the ligand (Fig. 1).

In Vitro Cytotoxicity of the Au(III)-Complex on the Growth of Healthy Cells (HDfn) and Cancer Cell Lines (A549)

The effect of the complex $[Au(L)Cl]Cl_2{\cdot}H_2O$ on the growth of A549 cells and on the growth of healthy cells (HDFn) was studied, and the half-inhibitory concentration of A549 and HDFn cells is determined and presented in Table 6 (Fig. S17). The highest percentage of inhibition of the complex was 51.69767% at a concentration of 400 μg/mL. In contrast, the minimal inhibition in the healthy cell line was 3.125% at 25 μg/mL.

The IC_{50} for $[Au(L)Cl]Cl_2{\cdot}H_2O$ in A549 cells was found to be 235.2 μg/mL, which is very low compared to the healthy cell line, which was 296.5 μg/mL. This is an excellent result because a much higher concentration is required to kill half of the healthy cells. This finding suggests that the complex $[Au(L)Cl]Cl_2{\cdot}H_2O$ could be a novel treatment for this type of cancer.

■ CONCLUSION

The spectroscopic studies and analytical data of the metal complexes of Cu(II), Ag(I), and Au(III) demonstrated that the ligand acts as a tridentate chelating agent of the N,N,N type. The coordination process occurs via the nitrogen atom of the purine ring, the azo group, and the azomethine group. It was discovered that the Au(III) Nano-complex targets cancer cells with remarkable selectivity while sparing healthy cells. In summary, this complex may be a novel

medication for treating lung cancer cells (A549), and further research into its potential as a treatment for other malignancies, including breast and colon cancers, may be undertaken in the future.

■ ACKNOWLEDGMENTS

The authors would like to sincerely thank the Faculty of Education for Women's Department of Chemistry, Kufa University, for their assistance in completing this work. We would also like to thank the technical staff at the Chemistry Laboratory of the College of Education for Pure Science (Ibn al-Haitham), Baghdad University, for providing the necessary technical assistance and support during the experiments.

■ CONFLICT OF INTEREST

The writers have no conflicts of interest.

■ AUTHOR CONTRIBUTIONS

Majida Ibrahim Obaid conducted the experiment and wrote the manuscript. Ibtihal Kadhim Kareem and Wurood Ali Jaafar interpreted the measurement results and revised the manuscript. All authors approved the final version of this manuscript.

■ REFERENCES

[1] Zafar, W., Ashfaq, M., and Sumrra, S.H., 2023, A review on the antimicrobial assessment of triazole-azomethine functionalized frameworks incorporating transition metals, *J. Mol. Struct.*, 1288, 135744.

[2] Mohamed, A.R., 2024, Digging into biochemical and signal transduction of old drugs: Xanthines and their association to cancer, *ERU Res. J.*, 3 (1), 849–870.

[3] Park, S.Y., Kim, S.B., Wan, J., Felice, F., and Yi, K.H., 2024, Lipolytic agents for submental fat reduction: Review, *Skin Res. Technol.*, 30 (2), e13601.

[4] Kapri, A., Pant, S., Gupta, N., and Nain, S., 2022, Recent advances in the biological significance of xanthine and its derivatives: A review, *Pharm. Chem. J.*, 56 (4), 461–474.

[5] Yadav, K., Yadav, D., Bhandari, D.D., and Yadav, R., 2022, Identification of 1,3-(dimethyl/propyl)-8-susbtituted (cinnamic acid/furan) xanthine derivatives with anti-bronchospasmodic activity using *in silico* and *in vivo* techniques, *ChemistrySelect*, 7 (17), e202200377.

[6] Malík, M., and Tlustoš, P., 2022, Nootropics as cognitive enhancers: Types, dosage and side effects of smart drugs, *Nutrients*, 14 (16), 3367.

[7] Yu, H., Chen, X., Guo, X., Chen, D., Jiang, L., Qi, Y., Shao, J., Tao, L., Hang, J., Lu, G., Chen, Y., and Li, Y., 2023, The clinical value of serum xanthine oxidase levels in patients with acute ischemic stroke, *Redox Biol.*, 60, 102623.

[8] Chang, B., Niu, C., and Jiang, Y., 2024, Xanthine or hypoxanthine or both may play therapeutical effect in Parkinson's disease through the endocannabinoid system, *Med. Hypotheses*, 182, 111231.

[9] Lee, Y., Hwang, J., Desai, S.H., Li, X., Jenkins, C., Kopp, J.B., Winkler, C.A., and Cho, S.K., 2022, Efficacy of xanthine oxidase inhibitors in lowering serum uric acid in chronic kidney disease: A systematic review and meta-analysis, *J. Clin. Med.*, 11 (9), 2468.

[10] Majhi, S., 2023, Recent developments in the synthesis and anti-cancer activity of acridine and xanthine-based molecules, *Phys. Sci. Rev.*, 8 (9), 2405–2439.

[11] Sherefedin, U., Belay, A., Gudishe, K., Kebede, A., Kumela, A.G., and Asemare, S., 2025, Photophysical properties of sinapic acid and ferulic acid and their binding mechanism with caffeine, *J. Fluoresc.*, 35 (4), 2379–2393.

[12] Khavari, F., Taheri, M., Manoochehri, H., Molaei, P., and Nouri, F., 2024, Evaluation of the combined effect of caffeine and 5-fluorouracil on colorectal cancer cell lines, *Asian Pac. J. Cancer Prev.*, 25 (4), 1419–1424.

[13] Gencoglu, H., Delioglu, S., Nergiz, M.A., Metin, R., Erten, F., Tokmak, M., Orhan, C., and Sahin, K., 2026, Synergistic effects of caffeine and paclitaxel in breast cancer cells: Mechanistic insights into NF-κB and Nrf2 signaling, *Cell Biochem. Funct.*, 44 (2), e70183.

[14] Peasah, E.B., Gyampoh, S., Kumar, S., Tanwieh, E.R., Nji, M.I., Asamoah, S., Neba, M C., Aba,

C.M.S., 2024, Investigation of the interaction between xanthines and commercial antimicrobials on selected microbes, *ISAR J. Med. Pharm. Sci.*, 2 (6), 24–33.

[15] Yani, M.A.O., Ali, T.F.S., Beshr, E.A.M., Hayallah, A.M., 2024, Recent innovations in biological activities of xanthine and its derivatives: A review, *S. Sphinx J. Pharm. Med. Sci.*, 8 (1), 19–39.

[16] Ali, S.A., Elzawi, N.R., and Elyassiry, A.M., 2021, Synergistic and antagonistic effects of azo-Schiff base with some antibiotics on Gram-positive bacterial isolates, *Res. Rev.: J. Microbiol. Virol.*, 11 (2), 25–31.

[17] Ashoor, L.S., Majeed, R.A., and Al-Shemary, R.K.R., 2021, Applications of biological of azo-Schiff base ligand and its metal complexes and: A review, *Muthanna J. Pure Sci.*, 8 (1), 74–90.

[18] Mohammed, K.F., and Hasan, H.A., 2022, Synthesis, chemical and biological activity studies of azo-Schiff base ligand and its metal complexes, *Chem. Methodol.*, 6 (12), 905–913.

[19] Mandal, P., 2024, Synthesis, characterization and a few noticeable properties of Ni(II) complexes embedded with azo (-N=N-) and azomethine (-C=N-) ligands: A brief review, *Chem. Rev. Lett.*, 7 (1), 65–122.

[20] Ispir, E., Ikiz, M., Inan, A., Sünbül, A.B., Tayhan, S.E., Bilgin, S., Köse, M., and Elmastaş, M., 2019, Synthesis, structural characterization, electrochemical, photoluminescence, antiproliferative and antioxidant properties of Co(II), Cu(II) and Zn(II) complexes bearing the azo-azomethine ligands, *J. Mol. Struct.*, 1182, 63–71.

[21] Elbadawy, H.A., Eldissouky, A., El-Apasery, M.A., Elsayed, D.S., and Alaswad, E.A., 2025, Synthesis, characterization, computational and dyeing behavior of Cu(II) and Zn(II) metal complexes derived from azo-Schiff bases containing phenol derivatives, *BMC Chem.*, 19 (1), 207.

[22] Obaid, H.T., Kadhum, M.Y., and Abdulnabi, A.S., 2022, Azo Schiff base derived from 2-hydroxy-1-naphthaldehyde as corrosion inhibitors for carbon steel in HCl medium: Experimental and theoretical studies, *Mater. Today: Proc.*, 60 (Pt. 3), 1394–1401.

[23] Mahdi, D.M., and Naser, A.W., 2024, Synthesis, characterizations, biological activity and molecular docking study of new azo Schiff -bases, *Adv. J. Chem. A*, 7 (6), 842–852.

[24] Menati, S., Azadbakht, R., Rudbari, H.A., and Bruno, G., 2021, Synthesis and characterization of four new azo-Schiff base and their nickel(II) complexes, *Polyhedron*, 205, 115296.

[25] Adnan, S., Al-Adilee, K.J., and Abedalrazaq, K.A., 2020, Synthesis, spectral characterization and anticancer studies of novel azo Schiff base and its complexes with Ag(I), Au(lll) and Pt(lV) ions, *Egypt. J. Chem.*, 63 (12), 4749–4756.

[26] Slassi, S., El-Ghayoury, A., Aarjane, M., Yamni, K., and Amine, A., 2020, New copper(II) and zinc(II) complexes based on azo Schiff base ligand: Synthesis, crystal structure, photoisomerization study and antibacterial activity, *Appl. Organomet. Chem.*, 34 (3), e5503.

[27] Rafique, S., Idrees, M., Nasim, A., Akbar, H., Athar, A., 2010 Transition metal complexes as potential therapeutic agents, *Biotechnol. Mol. Biol. Rev.*, 5 (2), 38–45.

[28] Shumi, G., Desalegn, T., Demissie, T.B., Ramachandran, V.P., and Eswaramoorthy, R., 2022, Metal complexes in target-specific anticancer therapy: Recent trends and challenges, *J. Chem.*, 2022 (1), 9261683.

[29] Doostmohammadi, A., Jooya, H., Ghorbanian, K., Gohari, S., and Dadashpour, M., 2024, Potentials and future perspectives of multi-target drugs in cancer treatment: The next generation anti-cancer agents, *Cell Commun. Signaling*, 22 (1), 228.

[30] Puzzo, M., De Santo, M., Morelli, C., Leggio, A., and Pasqua, L., 2024, The advent of molecular targeted therapies against cancer. Toward multi-targeting drugs through materials engineering: A possible future scenario, *Small Sci.*, 4 (8), 2400113.

[31] Kareem, I.K., and Hadi, M.A., 2020, Synthesis and characterization of some transition metal complexes with new azo-Schiff base ligand 3,4-bis(((1*E*,2*E*)-2-((2-((4-((*Z*)-(3-hydroxyphenyl)diazenyl)naphthalen-1-

yl)amino)ethyl)imino)-1,2-diphenylethylidene)amino)phenyl)(phenyl)methanone, *Egypt. J. Chem.*, 63 (1), 301–313.

[32] Jawad, S.A.A., and Kareem, I.K., 2022, Synthesis, characterization and biological study of open multi dentate new azo-Schiff ligand and it's divalent metal ion complexes with copper, zinc and mercury, *AIP Conf. Proc.*, 2386 (1), 030014.

[33] Sherif, S., Aboelnaga, A., Elshemy, N.S., Elabbadya, S., and Ramadan, S.K., 2026, Design and synthesis of novel sulfa-azo dyes: A sustainable approach to textile dyeing combined with microwave energy, *RSC Adv.*, 16 (6), 5374–5400.

[34] Al-adilee, K.J., and Hessoon, H.M., 2019, Synthesis, spectral properties and anticancer studies of novel hetrocyclic azo dye ligand derived from 2-amino-5-methyl thiazole with some transition metal complexes, *J. Phys.: Conf. Ser.*, 1234 (1), 012094.

[35] Noor, S.S., and Kareem, I.K., 2024, Exploring the anticancer activity of gold complex with newly ligand (DDIBM): Synthesis, spectral identification and magnetic susceptibility of its metallic complexes, *Indones. J. Chem.*, 24 (3), 822–834.

[36] Kyhoiesh, H.A.K., and Hassan, H.M., 2024, Synthesis, characterization, *in silico* DFT, molecular docking, ADMET profiling studies and toxicity predictions of Ag(I) complex derived from 4-aminoacetophenone, *ChemistrySelect*, 9 (4), e202304429.

[37] Sami, S., and Shaalan, N., 2024, Synthesis, structure, and biological activity studies of new metal ion complexes based on 3-[(3-hydroxynaphthalene-2-yl-ethylidene)-hydrazono]-1,3-dihydro-indol-2-one, *Indones. J. Chem.*, 24 (2), 370–378.

[38] Hussein, N.A., and Abbas, A.K., 2022, Synthesis, spectroscopic characterization and thermal study of some transition metal complexes derived from caffeine azo ligand with some of their applications, *J. Med. Pharm. Chem. Res.*, 4 (1), 67–93.

[39] Obaid, M.I., and Jaafar, W.A, 2022, Formation, characterization and thermal study of novel Schiff base ligand from sulfonic acid and its complexes with Co(II), Ni(II), Cu(II), Zn(II) and Hg(II) type NO, *Chem. Methodol.*, 6 (6) 457–462.

[40] Ali, A.M., and Hassani, Z.R., 2020, Preparation and characterization of new azo ligand and some of its chelate complexes, *J. Kufa Chem. Sci.*, 2 (6), 13–23.

[41] Hilal, T.A.A., and Kareem, I.K., 2025, Synthesis of some metal complexes with new heterocyclic ligand (5-(((2-(3-(1*H*-indol-3-yl)acryloyl)phenyl)amino)methylene)-2-thiooxodihydropyrimidine-4,6(1*H*,5*H*)-dione) and their biological effectiveness as antioxidant and anti-cancer, *Indones. J. Chem.*, 25 (1), 60–75.

[42] Jaafar, W.A, and Saeed, R.S., 2020, Synthesis, characterization and corrosion inhibition study of new heterocyclic compounds and Schiff base with [Co (II), Ni (II), Cu (II) and Hg (II)] complexes, *Syst. Rev. Pharm.*, 11 (10), 134–143.

[43] Al-Hasnawi, F., Abdul Karem, L.K., and Mortatha, D.M., (2023). Synthesis, physicochemical elucidation and biological screening study of new ligand derived from 5,6-*O*-isopropylidene-L-ascorbic acid and its metal(II) complexes, *Malays. J. Sci.*, 42 (3), 45–55.

[44] Radhi, S.M.J., Kareem, I.K., and Majeed, N.S., 2023, Preparation and characterization of new mixed ligand complexes for some transition metal ions (bivalent) with Schiff-Mannich and Schiff base ligands, *J. Kufa Chem. Sci.*, 3 (1), 1–25.

[45] Yahya, W.I., Mgheed, T.H., and Kadhium, A.J., 2022, Preparation, characterization of some metal complexes of new mixed ligands derived from 5-methyl imidazole and study the biological activity of palladium(II) complex as anticancer, *NeuroQuantology*, 20 (1), 71–83.

[46] Mohd Makhtar, S.N.N., Abd Hamed, N.K., and bin Hamdan, M.A.H., 2024, "Morphological analysis of photocatalytic membrane (SEM, FESEM, TEM)" in *Advanced Ceramics for Photocatalytic Membranes*, Elsevier, Amsterdam, Netherlands, 221–238.

[47] Aziz, A., Shaikh, H., Abbas, A., Zehra, K., and Javed, B., 2025, Microscopic techniques for nanomaterials characterization: A concise review, *Microsc. Res. Tech.*, 88 (5), 1599–1614.

[48] Yasir, A.F., and Jamel, H.O., 2023, Synthesis of a new DPTYEAP ligand and its complexes with their

assessments on physical properties, antioxidant, and biological potential to treat breast cancer, *Indones. J. Chem.*, 23 (3), 796–808.

[49] Ali, A., Chiang, Y.W., and Santos, R.M., 2022, X-ray diffraction techniques for mineral characterization: A review for engineers of the fundamentals, applications, and research directions, *Minerals*, 12 (2), 205.

[50] El-Boraey, H.A., and El-Domiaty, A.M., 2021, Influences of γ-ray irradiation on physico-chemical, structural, X-ray diffraction, thermal and antimicrobial activity of some γ-irradiated *N*′,*N*‴-((*Z*)-ethane-1,2-diylidine)bis(2-aminobenzohydrazide) metal complexes, *Appl. Radiat. Isot.*, 174, 109774.

[51] Nasiri, S., Rabiei, M., Palevicius, A., Janusas, G., Vilkauskas, A., Nutalapati, V., and Monshi, A., 2023, Modified Scherrer equation to calculate crystal size by XRD with high accuracy, examples Fe_2O_3, TiO_2 and V_2O_5, *Nano Trends*, 3, 100015.

[52] Fatimah, S., Ragadhita, R., Al Husaeni, D.F., and Nandiyanto, A.B.D., 2021, How to calculate crystallite size from X-ray diffraction (XRD) using Scherrer method, *Asean J. Sci. Eng.*, 2 (1), 65–76.

[53] Kyhoiesh, H.A.K., and Al-Adilee, K.J., 2023, Pt(IV) and Au(III) complexes with tridentate-benzothiazole based ligand: Synthesis, characterization, biological applications (antibacterial, antifungal, antioxidant, anticancer and molecular docking) and DFT calculation, *Inorg. Chim. Acta*, 555, 121598.

[54] Kyhoiesh, H.K.A., and Al-Adilee, K.J., 2021, Synthesis, spectral characterization, antimicrobial evaluation studies and cytotoxic activity of some transition metal complexes with tridentate (N,N,O) donor azo dye ligand, *Results Chem.*, 3, 100245.